INSTITUTE OF PHYSICS PUBLISHING NANOTECHNOLOGY

Nanotechnology **15** (2004) 1–8 PII: S0957-4484(04)65726-6

Bandstructures of conical quantum dots with wetting layers

R V N Melnik[1] **and M Willatzen**

Mads Clausen Institute for Product Innovation, University of Southern Denmark, Grundtvigs Alle 150, DK-6400 Sønderborg, Denmark

E-mail: rmelnik@mci.sdu.dk

Received 8 July 2003, in final form 22 September 2003
Published 10 November 2003
Online at stacks.iop.org/Nano/15/1 (DOI: 10.1088/0957-4484/15/1/001)

Abstract

The influence of wetting-layer states on quantum-dot states and vice versa is analysed numerically for electrons in the conduction band in the general case with arbitrary kinetic energy in the plane of the quantum-well wetting layer. Since the analysed quantum dot is embedded in a barrier material with different properties, the effective mass approximation methodology leads to a Schrödinger model with discontinuous coefficients. This complicates the analysis and, in addition, requires a special attention to the formulation of boundary conditions for the entire structure, consisting of the quantum dot with wetting layer embedded in a barrier material. In the present paper, the complete model is formulated and solved numerically via a variational approach based on finite element approximations and Arnoldi iterations. By analysing different geometrical configurations, we demonstrate that the ground eigenstate of the entire structure can be considerably affected by the presence of the wetting layer. The dependency demonstrated between eigenstates of the 'pure' quantum dots and the quantum-well wetting layers indicates that a conventional analysis of quantum-dot structures without accounting for wetting layers may not be sufficient for an adequate characterization of quantum dots as active regions in future electronic and optical devices.

1. Introduction

It is known experimentally that three-dimensional confinement of electrons is possible within strained islands formed by pseudomorphic growth of a thin layer of a material, e.g. InAs, on a GaAs (100) substrate during the Stranski–Krastanow growth method [1–7]. Due to the lattice mismatch between the deposited material and the substrate, after a certain thickness is reached, strain effects lead to the formation of (pyramidal) quantum dots above a thin quantum-well wetting layer. Although bandstructure analyses have been performed for 'pure' quantum dots of various topologies (e.g. [8, 9] and references therein), a systematic analysis of the influence of the wetting layer on electronic states of the entire structure has not been reported in the literature. Some preliminary results of this analysis have recently been announced in [7]. Here we provide a complete formulation of the model for this analysis and discuss a numerical methodology for obtaining eigenstates of quantum dots with wetting layers.

It is essential to obtain a better understanding of electron states in these combined quantum-dot/wetting-layer structures in order to assess the importance of carrier relaxation and dephasing time effects for the performance of optoelectronic devices where semiconductor quantum dots form the active region [10, 11].

In the present work, a model for electrons confined to the InAs region of self-assembled InAs/GaAs quantum-dot structures with wetting layers is examined based on the $\vec{k} \cdot \vec{p}$ method. Previous works that use the $\vec{k} \cdot \vec{p}$ theory for the analysis of self-assembled quantum-dot structures with wetting layers either decouple the higher energy states (those not decaying away from the quantum-dot region) from the bound states in a multiband strain Hamiltonian bandstructure analysis [3, 12–16] or rely on the Bloch periodicity in the 'crystal' formed by an infinite set of regularly spaced quantum dots above an infinite

[1] Author to whom any correspondence should be addressed.

quantum-well wetting layer [17]. The purpose of the current paper is to present a general methodology that can be applied to both isolated and coupled quantum dots of arbitrary shape in the presence/absence of a wetting layer. We have chosen to present results for the simple one-band model case although the proposed numerical model can be extended in principle to multiband $\vec{k} \cdot \vec{p}$ Hamiltonian problems. In the numerical experiments presented in this paper, the pyramidal quantum-dot structures observed experimentally are approximated by cones. This assumption is not expected to affect the general physics as to the influence of wetting layers on quantum-dot states or vice versa. However, it does allow us to reduce the original model to two dimensions by using cylindrical coordinates and, hence, to reduce substantially computational efforts required for the problem solution.

The model presented accounts for states with an arbitrary kinetic energy in the quantum-well wetting layer. Electron states corresponding to a single quantum-dot structure with a wetting layer will asymptotically approach either (a) 'pure' quantum-well states far away from the quantum-dot region or (b) zero if the state is a 'true' quantum-dot state. We employ this fact to formulate general boundary conditions for the combined quantum-dot/wetting-layer structure to be analysed numerically.

2. Theory

In the following, a general model and a numerical procedure for its discretization, allowing us to determine electronic eigenstates and associated eigenvalues of any cylindrically symmetric quantum-dot structure with the possible inclusion of wetting layers, will be described. The starting point is the one-band Schrödinger equation in the effective mass approximation:

$$-\frac{\hbar^2}{2}\nabla\cdot\left(\frac{1}{m_{\mathrm{e}}(\vec{x})}\nabla\psi(\vec{x})\right)+V_{\mathrm{e}}(\vec{x})\psi(\vec{x})=E\psi(\vec{x}), \qquad (1)$$

where $\hbar$, $m_{\mathrm{e}}(\vec{z})$, $V_{\mathrm{e}}(\vec{z})$, E, and $\psi(\vec{z})$ are Planck's constant divided by 2π, the position-dependent electron effective mass, the position-dependent band-edge potential energy, the electron energy, and the electron envelope function, respectively. Note that the methodology developed in this paper is extendable to multiband Schrödinger models but, in what follows, we will focus on the one-band model only.

Since cylindrical symmetry is assumed, we have that $\vec{x}=(z,r,\phi)$ where z is the axial co-ordinate, r is the radial co-ordinate, and ϕ is the azimuthal angle in the range 0–2π ($V_{\mathrm{e}}(\vec{x})=V_{\mathrm{e}}(z,r)$ and $m_{\mathrm{e}}(\vec{x})=m_{\mathrm{e}}(z,r)$). Assuming that $\psi(\vec{x})$ has a separable form in ϕ

$$\psi(\vec{x})=\chi(z,r)\Phi(\phi), \qquad (2)$$

equation (1) becomes

$$\begin{aligned}&-\frac{\hbar^2}{2}\frac{\partial}{\partial z}\left(\frac{1}{m_{\mathrm{e}}(z,r)}\frac{\partial\chi}{\partial z}\right)\Phi(\phi)-\frac{\hbar^2}{2}\frac{1}{r}\frac{\partial}{\partial r}\left(\frac{r}{m_{\mathrm{e}}(z,r)}\frac{\partial\chi}{\partial r}\right)\Phi(\phi)\\&\quad-\frac{\hbar^2}{2m_{\mathrm{e}}(z,r)}\frac{\chi(z,r)}{r^2}\frac{\partial^2\Phi}{\partial\phi^2}+V_{\mathrm{e}}(z,r)\chi(z,r)\Phi(\phi)\\&\quad=E\chi(z,r)\Phi(\phi). \qquad (3)\end{aligned}$$

Dividing equation (3) by $\frac{\Phi\chi}{m_{\mathrm{e}}(z,r)r^2}$ and rearranging leads to

$$\begin{aligned}&m_{\mathrm{e}}(z,r)r^2\left(-\frac{\hbar^2}{2}\frac{\partial}{\partial z}\left(\frac{1}{m_{\mathrm{e}}(z,r)}\frac{\partial\chi_n}{\partial z}\right)\frac{1}{\chi_n(z,r)}\right.\\&\quad\left.-\frac{\hbar^2}{2}\frac{1}{r}\frac{\partial}{\partial r}\left(\frac{r}{m_{\mathrm{e}}(z,r)}\frac{\partial\chi_n}{\partial r}\right)\frac{1}{\chi_n(z,r)}\right)\\&\quad+m_{\mathrm{e}}(z,r)r^2(V_{\mathrm{e}}(z,r)-E)=\frac{\hbar^2}{2}\frac{\partial^2\Phi}{\partial\phi^2}\frac{1}{\Phi(\phi)}\equiv-\frac{\hbar^2}{2}n^2.\end{aligned} \qquad (4)$$

The last expression for $\Phi(\phi)$ in equation (4) can be solved immediately to give

$$\Phi(\phi)=\exp(\mathrm{i}n\phi), \qquad (5)$$

where n is an integer for Φ to be a single-valued function: $\Phi(0)=\Phi(2\pi)$. The remaining part of equation (4) can be written as

$$\begin{aligned}&-\frac{\hbar^2}{2}\frac{\partial}{\partial z}\left(\frac{1}{m_{\mathrm{e}}(z,r)}\frac{\partial\chi_n}{\partial z}\right)-\frac{\hbar^2}{2}\frac{1}{r}\frac{\partial}{\partial r}\left(\frac{r}{m_{\mathrm{e}}(z,r)}\frac{\partial\chi_n}{\partial r}\right)\\&\quad+\frac{\hbar^2}{2m_{\mathrm{e}}(z,r)}\frac{n^2}{r^2}\chi_n(z,r)+V_{\mathrm{e}}(z,r)\chi_n(z,r)=E\chi_n(z,r).\end{aligned} \qquad (6)$$

The original model (1) as well as the derived model (6) have discontinuous coefficients under spatial derivative operators due to different material properties in the quantum-dot/wetting-layer structure and the barrier. Therefore, both models should be understood in a generalized sense and, strictly speaking, should be re-formulated in the form of integral equations. From a physical point of view, one has to view the original model (1) (and, similarly, equation (6)) as one where the following two conditions should be satisfied (e.g. [9])

$$\psi(\vec{x})\in C(Q), \qquad -1/m_{\mathrm{e}}^{\mathrm{s}}\nabla\psi(\vec{x})\cdot\vec{n}=1/m_{\mathrm{e}}^{\mathrm{b}}\nabla\psi(\vec{x})\cdot\vec{n}, \qquad (7)$$

where $m_{\mathrm{e}}(\vec{x})=m_{\mathrm{e}}^{\mathrm{s}}$ is the electron effective mass in the quantum-dot/wetting-layer structure, $m_{\mathrm{e}}(\vec{x})=m_{\mathrm{e}}^{\mathrm{b}}$ is the electron effective mass in the barrier material, Q is the spatial (r,z) domain of interest, C is the class of continuous functions, and $\vec{n}$ is outer normal vector in the domain under consideration. Under these circumstances numerical methodologies based on a variational re-formulation of the governing equations stated above become a natural tool in the analysis of these low-dimensional semiconductor structures as soon as realistic geometries and the presence of the wetting layer are taken into consideration.

The envelope function solution for a stepwise constant effective mass $m_{\mathrm{e}}(z)\equiv m_{\mathrm{e}}(z,r)$ and potential $V_{\mathrm{e}}(z)\equiv V_{\mathrm{e}}(z,r)$ (the so-called 'pure' wetting-layer case),

$$m_{\mathrm{e}}(z)=\begin{cases}m_w & \text{if } -L/2\leqslant z\leqslant L/2\\ m_b & \text{if } z\leqslant -L/2 \text{ or } z\geqslant L/2,\end{cases} \qquad (8)$$

$$V_{\mathrm{e}}(z)=\begin{cases}0 & \text{if } -L/2\leqslant z\leqslant L/2\\ V & \text{if } z\leqslant -L/2 \text{ or } z\geqslant L/2,\end{cases} \qquad (9)$$

is [18]

$$\psi_{nk}(z,r,\phi)=A_{nk}Z_{nk}(z)J_n(kr)\exp(\mathrm{i}n\phi), \qquad (10)$$

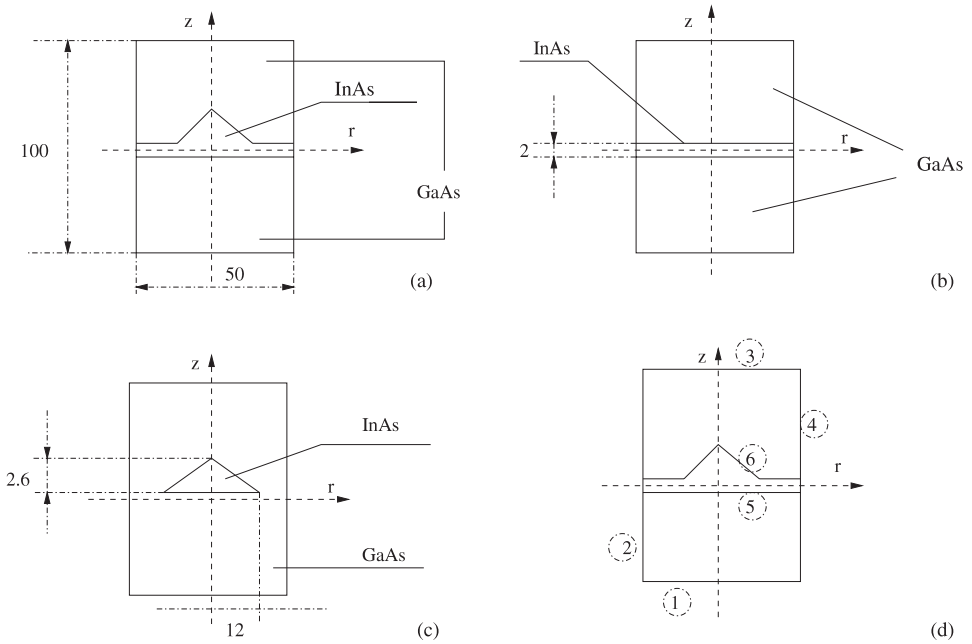

Figure 1. Geometries and zone boundary edges: (a) full quantum-dot/wetting-layer structure; (b) 'pure' wetting layer; (c) 'pure' quantum dot; (d) zone boundary edges.

where Z_{nk} is a solution to

$$\frac{\partial}{\partial z}\left(\frac{1}{m_e(z)}\frac{\partial Z_{nk}}{\partial z}\right)+\frac{2}{\hbar^2}\left(E-V_e(z)-\frac{\hbar^2k^2}{2m_e(z)}\right)Z_{nk}=0. \quad (11)$$

It follows immediately that ψ_{nk} also satisfies

$$\frac{\partial\psi_{nk}}{\partial r}-\frac{1}{2}\frac{k(J_{n-1}(kr)-J_{n+1}(kr))}{J_n(kr)}\psi_{nk}=0, \quad \text{if } J_n(kr)\neq 0 \quad (12)$$

$$\psi_{nk}=0, \quad \text{if } J_n(kr)=0.$$

since

$$\frac{\partial J_n(y)}{\partial y}=\frac{1}{2}(J_{n-1}(y)-J_{n+1}(y)). \quad (13)$$

3. Boundary conditions and general numerical methodology

Before approaching the solution of (6), this rather general equation should be supplemented by appropriate boundary conditions. To derive physically adequate boundary conditions for the entire quantum-dot/wetting-layer structure is a far from trivial task. Firstly, let us consider geometries corresponding to the cylindrically symmetric quantum-dot structure with a quantum-well layer (wetting layer) as shown in figure 1(a). We define the z axis to be perpendicular to the plane of the quantum-well layer. The r axis then lies in the quantum-well plane (figure 1(a)). Figure 1(d) shows the computational region corresponding to the combined quantum-dot/wetting-layer structure with the boundaries numbered. On the boundaries 1 and 3, Dirichlet boundary conditions ($\psi = 0$) are imposed as we are only interested in electronic states confined to the quantum-dot and wetting-layer regions. Boundaries 5 and 6 are internal boundaries on which continuity of $\chi_n(z,r)$, $\frac{1}{m_e(z,r)}\frac{\partial\chi_n}{\partial z}$, and $\frac{r}{m_e(z,r)}\frac{\partial\chi_n}{\partial r}$ must be imposed (refer to equation (6)).

The relevant boundary conditions on boundaries 2 and 4 will be specified next. Note, however, that due to the symmetry of the problem, we can divide the computational region into two equal parts and replace boundary 2 by boundary 7 (dashed vertical line in figure 1(d)).

Boundary conditions on boundary 7 ($r = 0$) deserve special treatment. Clearly, when $n \geqslant 1$, Dirichlet conditions must be imposed at this symmetry line to ensure that the term $\frac{\hbar^2}{2m_e(z,r)}\frac{n^2}{r^2}\chi_n(z,r)$, appearing in equation (6), does not diverge at $r = 0$. However, when $n = 0$, this term disappears and instead Neumann boundary conditions must be employed to ensure that $\vec{\nabla}\psi$ exists at $r = 0$. The latter result follows from

$$\psi(z,r,\theta)=\psi(z,r,\theta+\pi), \quad (14)$$

if $n = 0$, and the fact that the slope of ψ along the r direction for any fixed values of z and θ can be written as:

$$\lim_{\epsilon\to 0}\frac{\psi(z,r=\epsilon,\theta)-\psi(z,r=0,\theta)}{\epsilon} = \lim_{\epsilon\to 0}\frac{\psi(z,r=0,\theta)-\psi(z,r=\epsilon,\theta+\pi)}{\epsilon}. \quad (15)$$

Boundary conditions at boundary 2 are determined using asymptotic arguments. At large r values, the envelope function for the combined quantum dot/wetting layer approaches asymptotically either (a) the envelope function for the 'pure' wetting-layer problem or (b) zero if the state is a 'true' quantum-dot state, i.e. equation (12) can be used as a boundary condition at boundary 4 (mixed boundary condition) for the combined quantum-dot/wetting-layer problem. This is so since boundary 4 is assumed to be located at a large value of r, denoted by R^*, far away from the quantum-dot region. In the examples that follow $R^* = 25$ nm (see figure 1(a)). This value satisfies the assumption made above.

Finally, before proceeding to the discussion of our numerical results, we make several remarks on discretization

of the model that has been developed and its computational implementation. From a mathematical point of view, model (6), supplemented by corresponding boundary conditions, is a partial differential equation (PDE) eigenvalue problem. Using finite element methodology (MATLAB-based FEMLAB), the problem is discretized and the corresponding algebraic eigenvalue problem, $(A - (E - V)I)\vec{\chi}_n = \vec{f}$ with given matrix A and $\vec{f}$, is solved with the spectral transformation Arnoldi iterations (e.g. [19, 20] and references therein)

$$K_m(A, \vec{\chi}_n) = \text{span}\{\vec{\chi}_n, A\vec{\chi}_n, \ldots, A^{m-1}\vec{\chi}_n\}. \qquad (16)$$

Note that the standard QR methodology, applied in the context of modelling quantum-dot nanostructures in [8, 21], destroys the sparcity of the matrix. At each iteration k of the QR method we need to overwrite the vector $A^{k-1}\vec{\chi}_n$ with $A^k\vec{\chi}_n$, while in the methodology applied in this paper we keep the entire set of previous vectors $\{\vec{\chi}_n, A\vec{\chi}_n, \ldots, A^{m-1}\vec{\chi}_n\}$. The subspace (16) is the mth order Krylov subspace that corresponds to the matrix A and vector $\vec{\chi}_n$, and approximate eigenvectors are constructed here in this subspace. More precisely, an approximation to eigenpairs of the problem, $(\vec{\psi}_i, E_i)$, is constructed as Ritz pairs that satisfy the Galerkin condition which gives the eigenvector–eigenvalue relationship in the projection on to a smaller space

$$\vec{v}^T(A\vec{\psi}_i - E_i\vec{\psi}_i) = 0 \qquad (17)$$

with $\vec{v}$ being an arbitrary vector from the subspace $K_m(A, \vec{\chi}_n)$. To ensure a high accuracy of the results, computations were carried out on a sequence of grids with the number of nodes ranging from 10 000 to 50 000. This procedure ensures that the difference between the results obtained on two subsequent grids is negligible. In particular, in all computational experiments, the initial grid was first refined in the domain of the quantum dot/wetting layer. Then, computations were performed by implementing a mesh refinement procedure for the complete domain, including the barrier material. The results reported in the next section were obtained after the complete domain was refined three times and computational errors were minimized. In particular, all results reported here remain the same after further mesh refinement. Finally, note that we specified explicitly the range of computed eigenvalues within the limit given by the barrier energy level. This simple modification, motivated by the physics of the problem, allowed us to reduce the computational cost of solving the problem.

4. Numerical results and discussions

As a first step, we computed the bandstructure (k, E_n) for the 'pure' wetting-layer or quantum-well problem (figure 1(b)). In figure 2 (upper plot), the bandstructure for $n = 0$ is shown. It is evident that four different states are captured below the barrier potential of 0.697 eV. These four subbands do *not* represent four different subbands in the usual sense, i.e. corresponding to 0, 1, 2, and 3 nodes along the z direction. Rather, they represent the four possible solutions for the wavefunction that satisfy the boundary conditions on the surfaces of constant r with energies below the barrier potential, i.e. waves with 0, 1, 2, and 3 nodes along the r direction. The computed energy eigenvalue of the state without nodes in the r direction is 0.385 eV at $k = 0$ which is in perfect agreement with analytical results [18].

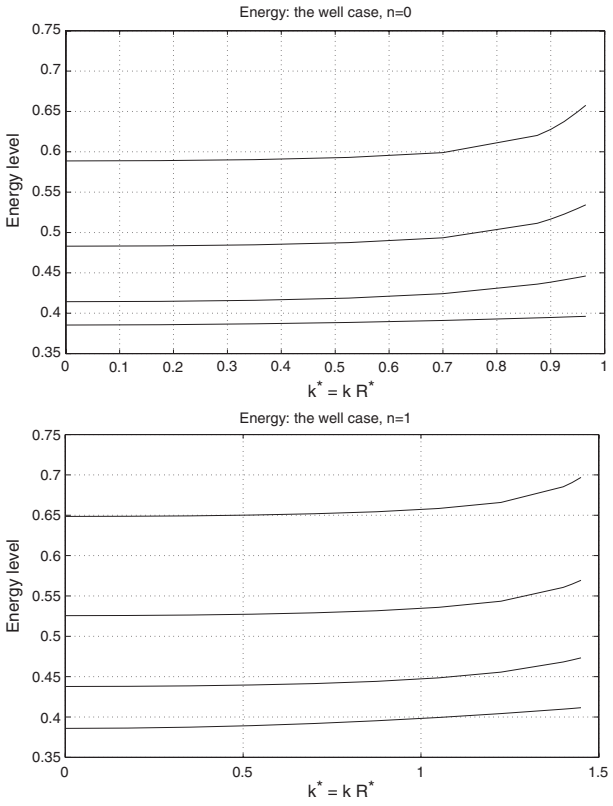

Figure 2. k^*–E dispersion relations for the 'pure' wetting layer depicted in figure 1(b) in the case $n = 0$ (upper plot) and $n = 1$ (lower plot). Axis labels are $k^* = kR^*$ (dimensionless) for the first axis with $R^* = 25$ nm and energies in electronvolts for the second axis.

Secondly, we computed the bandstructure for the 'pure' wetting-layer problem in the case $n = 1$ and obtained, similarly to the case above, four subbands in the energy interval 0–0.697 eV (figure 2 (lower plot)). Only one 'true' subband exists, i.e. all confined states have 0 nodes along the z direction. The four subbands have 0, 1, 2, and 3 nodes along the r direction. The computed energy eigenvalue of the state without nodes in the r direction is 0.386 eV at $k = 0$. This again is in perfect agreement with analytical results [18].

Next, we computed dispersion relations for the conical dot case with no quantum-well wetting layer. Based on these results, we observed that when $n = 0$ two states are confined to the InAs quantum dot. The energies of both states (0.48 and 0.69 eV) are independent of k, reflecting the fact that these states are true quantum-dot states. In other words, their wavefunctions decrease exponentially in the GaAs region away from the InAs quantum dot and are zero at boundary 4. Any state vanishing at boundary 4 must be independent of k since k appears in the computations only through the boundary condition at interface 4. The ground-state envelope function is shown in figure 3 (0.48 eV). Note that wavefunctions can be non-zero at the centre of the quantum dot only for $n = 0$, due to the presence of the term $\frac{\hbar^2}{2m_e(z,r)}\frac{n^2}{r^2}\chi_n(z, r)$ in equation (6), as mentioned earlier. It can be seen in figure 4 that the second state (first excited state) has a very small albeit non-vanishing

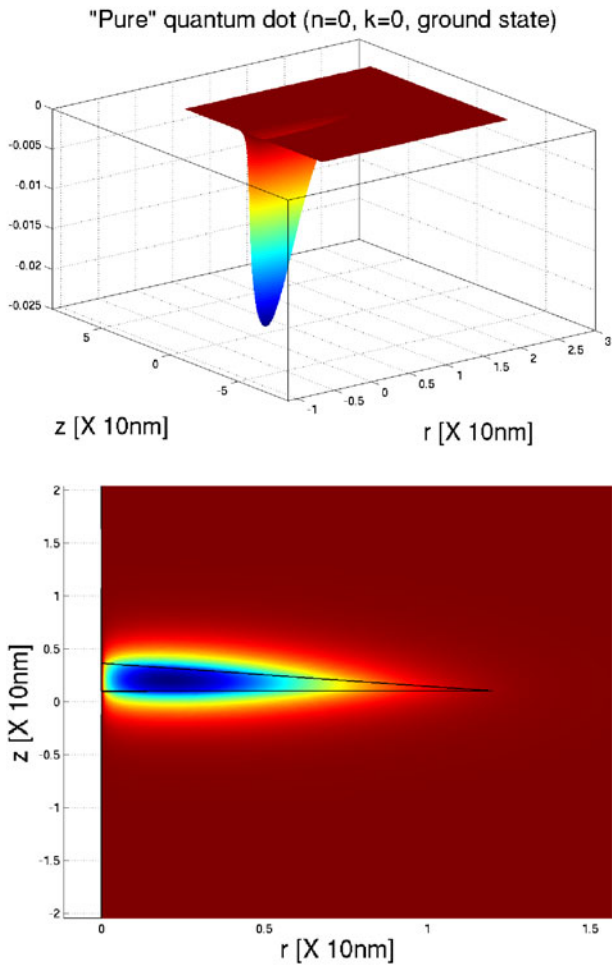

Figure 3. The ground-state envelope function for the 'pure' quantum dot plotted against z and r coordinates in the case $n = 0, k = 0$. Dimensional lengths are in units of 10 nm. The upper (lower) plot is a three-dimensional (contour) plot of the ground-state envelope function.

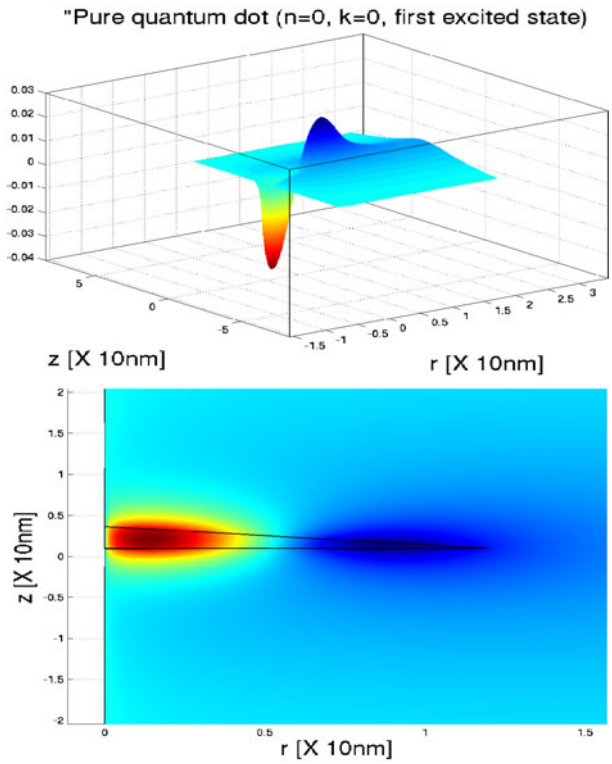

Figure 4. The envelope function of the first excited state for the 'pure' quantum dot plotted against z and r coordinates in the case $n = 0, k = 0$. Axis labels are as in figure 3. The upper (lower) plot is a three-dimensional (contour) plot of the ground-state envelope function.

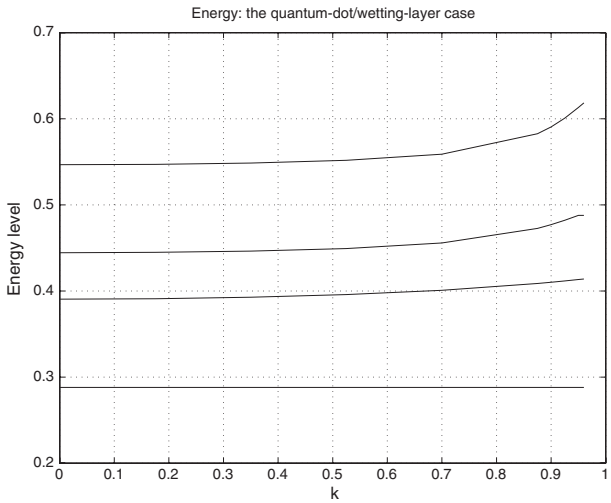

Figure 5. k^*–E dispersion relations for the combined quantum-dot/wetting-layer structure depicted in figure 1(a) in the case $n = 0$ ($k^* = kR^*$ with $R^* = 25$ nm). Axis labels are as in figure 2.

wavefunction at the boundary 4. This agrees with the fact that the energy of this state (0.69 eV) is close to the barrier energy (0.697 eV) making the second state a weakly confined quantum-dot state.

In the conical dot case with no wetting layer for $n = 1$ only one confined state is found with energy 0.6046 eV independent of k. Thus, this state is a true quantum-dot state. The wavefunction for this state is zero at the centre of the quantum dot, as it must be, based on the argument in the preceding paragraph. The wavefunction vanishes at boundary 4 as required.

In figure 5, the dispersion relation for the combined dot and wetting-layer structure is shown for $n = 0$. Four subbands are found and will be discussed next. The band with lowest energy is a quantum-dot state as it is nearly dispersion-free (the energies at $k = 0$ and 0.0875 are 0.288 03 and 0.288 04 eV, respectively). The associated wavefunction is shown in figure 6 for $k = 0$. As expected, the wavefunction is non-zero at the centre of the quantum dot and decays exponentially to zero at boundary 4 in the GaAs region. Although this state vanishes at boundary 4 and the associated energy dispersion curve is flat, the energy of this state, 0.288 eV, is very different from the 'pure' dot state energy, 0.48 eV (the latter wavefunction is shown in figure 3). It is observed that the ground-state wavefunction for the combined quantum-dot and wetting-layer structure is substantially different from zero in the wetting-layer region nearest to the quantum dot. This is obviously not the case for any state in the 'pure' quantum-dot case since there is no wetting-layer presence and the

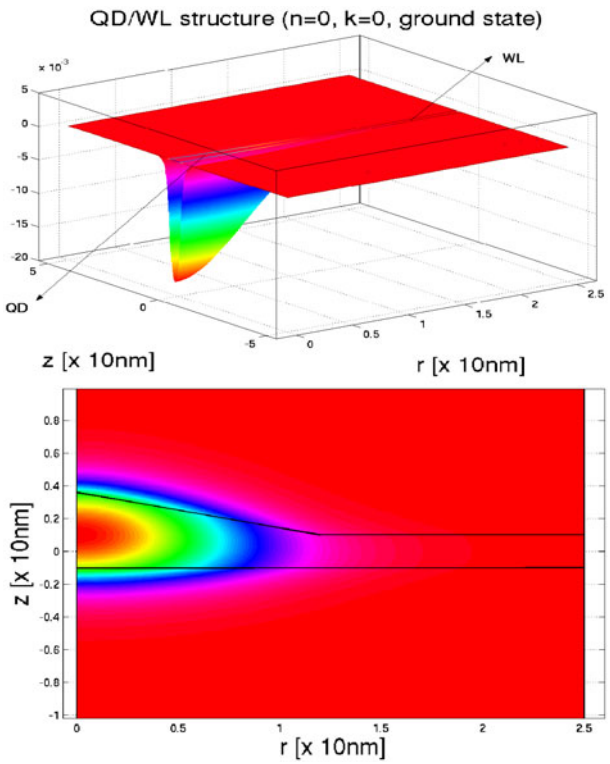

Figure 6. The ground-state envelope function of the combined quantum-dot/wetting-layer structure, as shown in figure 1(a), for $n = 0$, $k = 0$. Axis labels are as in figure 3.

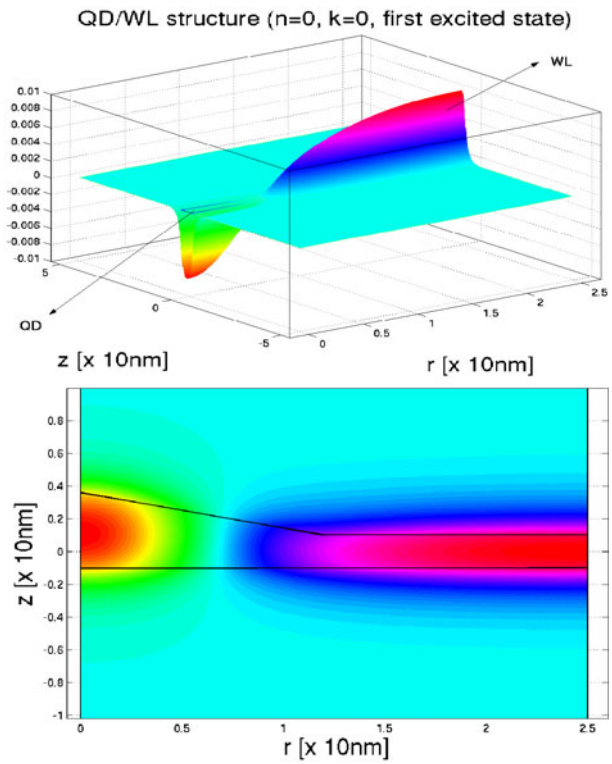

Figure 7. The envelope function of the first excited state for the combined quantum-dot/wetting-layer structure, as shown in figure 1(a), for $n = 0$, $k = 0$. Axis labels are as in figure 3.

associated wavefunction must decay immediately outside the quantum-dot region. Next, consider the second lowest state in figure 7. This state (shown at $k = 0$) is analogous to the second state for the 'pure' quantum-well case since both states have one node along the r direction. The energy of this second state is 0.390 eV. Similarly, the third and fourth band depicted in figure 5 have two and three nodes along the r direction, respectively. The corresponding energies are 0.444 and 0.547 eV.

Although our major concern is the formulation of a computational model able to describe electronic states in quantum-dot structures with wetting layers, we shall briefly discuss the implications of coupled quantum-dot/wetting-layer states for carrier capture processes in quantum dots [22]. An important aspect in device applications of quantum-dot structures with wetting layers is the possible existence of quasi-bound states characterized by envelope functions which satisfy the following inequality

$$\int_{V_{r\leqslant R}} |\chi_n(z)|^2 \,\mathrm{d}V \Big/ \int_{V_{r>R}} |\chi_n(z)|^2 \,\mathrm{d}V \gg \int_{V_{r\leqslant R}} \mathrm{d}V \Big/ \int_{V_{r>R}} \mathrm{d}V, \tag{18}$$

where R is the quantum-dot cone-base radius, and $V_{r\leqslant R}$ and $V_{r>R}$ refer to the volumes of the wetting-layer region just above the quantum-dot region and the rest of the wetting-layer (computational) zone, respectively. Such states are predominantly located in or above the quantum-dot region but they can have considerable tails away from the quantum-dot region, i.e. in the wetting-layer regions for which $r > R$. Hence, these states may lead to effective carrier coupling between the wetting-layer and quantum-dot regions. Such states are expected to form an important role in carrier capture from the wetting layer to the quantum dot through carrier–phonon and carrier–carrier scattering processes [23].

In figure 7, an envelope function is shown corresponding to a state where coupling between the wetting-layer region and the quantum-dot region exists, although the coupling is relatively weak. In other words, this state is more or less uniformly spread over the full wetting-layer region and the above inequality is not satisfied. To investigate this effect further, we extend the computational domain in the r-direction and look for states which are predominantly located at or above the quantum dot, but do not decay exponentially quickly in the wetting layer as r increases. One such state, being a higher excited state for this structure and satisfying the inequality (18), is shown in figure 8. This state may play a stronger role in relation to carrier capture processes due to its stronger presence close to the quantum-dot region.

In figure 9, the dispersion relation for the combined dot and wetting-layer structure is shown for $n = 1$. Again, the state associated with the lowest band (four subbands in total) is essentially a quantum-dot state—having zero nodes along the r direction—as the associated energy is almost independent of k. In fact, the energies of this state are 0.3671 and 0.3690 eV at $k = 0$ and 1.40, respectively. The corresponding wavefunction at $k = 1.40$ is shown in figure 10. Notice the non-zero slope of this wavefunction at boundary 4 as a result of the boundary condition given in equation (12). The remaining three subbands (located at higher energies) in

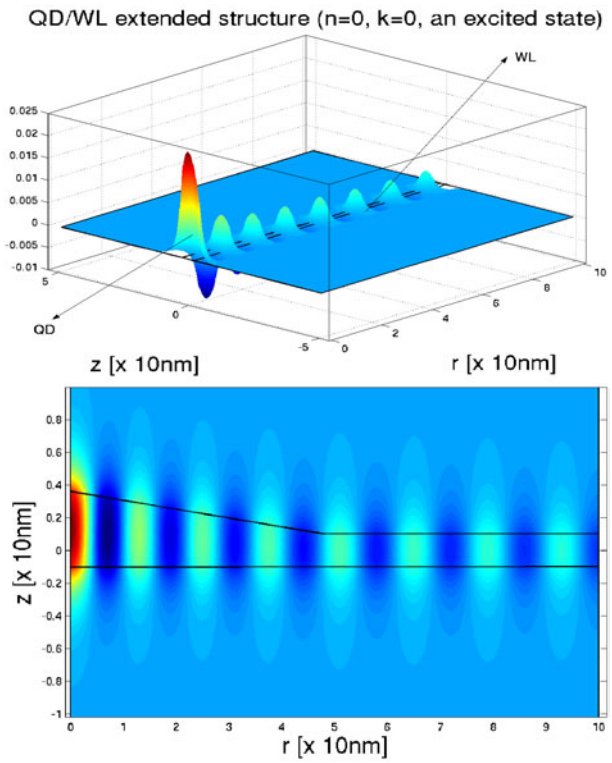

Figure 8. Coupled state in the quantum-dot/wetting-layer extended structure for $n = 0$, $k = 0$. Axis labels are as in figure 3.

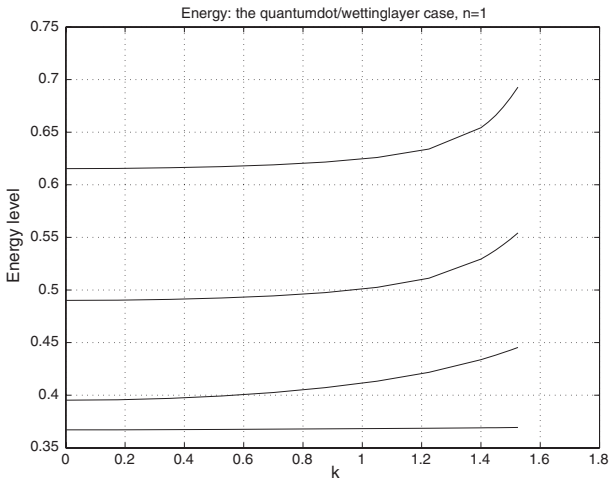

Figure 9. k^*–E dispersion relations for the combined quantum-dot/wetting-layer structure depicted in figure 1(a) in the case $n = 1$ ($k^* = kR^*$ with $R^* = 25$ nm). Axis labels are as in figure 2.

figure 9 correspond to the states having 1, 2, and 3 nodes along the r direction.

5. Conclusions

A model and a numerical procedure for its solution are proposed for determining eigenstates for self-assembled quantum-dot/wetting-layer structures. The pyramidal quantum-dot shapes observed experimentally are approximated by conical quantum dots since this allows a simplified two-dimensional

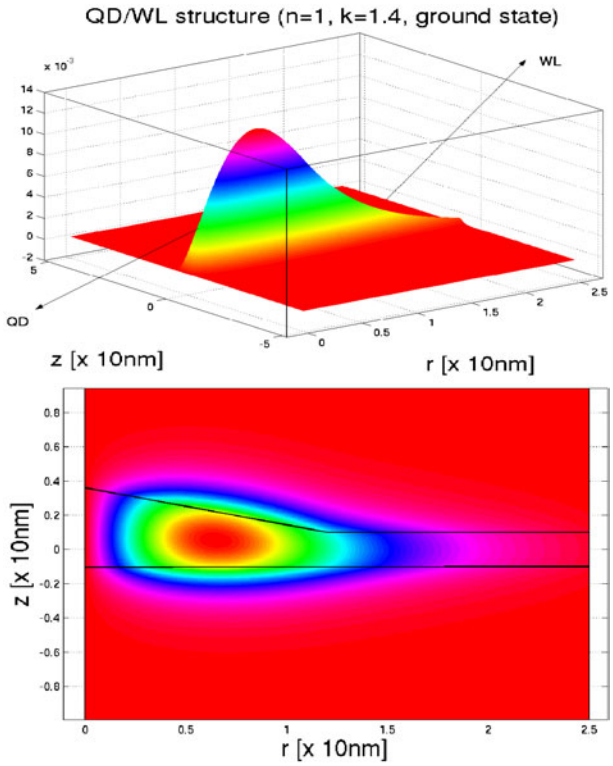

Figure 10. The ground-state envelope function for the combined quantum-dot/wetting-layer structure, as presented in figure 1(a), for $n = 1$, $k = 1.40$. Axis labels are as in figure 3.

computational treatment due to axisymmetry. Our major focus in this paper has been on studying *single* quantum dots above the quantum-well wetting layer. However, the developed methodology is easily extendable to other geometric configurations.

Boundary conditions corresponding to zone edges located far away from the quantum-dot region are found using the fact that electron states will asymptotically approach either (a) 'pure' quantum-well states far away from the quantum-dot region or (b) zero if the state is a 'true' quantum-dot state. Results are presented for the cases (a) the 'pure' quantum-well, (b) the 'pure' conical quantum dot, and (c) the combined quantum-dot/wetting-layer structure.

References

[1] Marzin J Y and Bastard G 1994 Calculation of the energy levels in InAs/GaAs quantum dots *Solid State Commun.* **92** 437–42

[2] Li S, Xia J, Yuan Z L, Xu Z Y, Ge W, Wang X R, Wang Y, Wang J and Chang L L 1996 Effective-mass theory for InAs/GaAs strained coupled quantum dots *Phys. Rev.* B **54** 11575–81

[3] Stier O, Grundmann M and Bimberg D 1999 Electronic and optical properties of strained quantum dots modeled by 8×8-band $k \cdot p$ theory *Phys. Rev.* B **59** 5688–701

[4] Grundmann M, Stier O and Bimberg D 1995 InAs/GaAs pyramidal quantum dots: strain distribution, optical phonons, and electronic structure *Phys. Rev.* B **52** 11969–81

[5] Jiang H and Singh J 1998 Self-assembled semiconductor structures: electronic and optoelectronic properties *IEEE J. Quantum Electron.* **34** 1188–96

[6] Califano M and Harrison P 2000 Presentation and experimental validation of a single-band, constant-potential model for self-assembled InAs/GaAs quantum dots *Phys. Rev.* B **61** 10959–65
[7] Melnik R V N and Willatzen M 2002 Modelling coupled motion of electrons in quantum dots with wetting layers *Technical Proc. 5th Int. Conf. on Modeling and Simulation of Microsystems, MSM 2002 (Puerto Rico, USA, April 2002)* (USA: ACRS) pp 506–9
[8] Li Y *et al* 2001 Computer simulation of electron energy levels for different shape InAs/GaAs semiconductor quantum dots *Comput. Phys. Commun.* **141** 66–72
[9] Gelbard F and Malloy K J 2001 Modeling quantum structures with BEM *J. Comput. Phys.* **172** 19–39
[10] Uskov A V, Jauho A-P, Tromborg B, Mørk J and Lang R 2000 Dephasing times in quantum dots due to elastic LO phonon–carrier collisions *Phys. Rev. Lett.* **85** 1516–9
[11] Borri P, Langbein W, Mørk J, Hvam J M, Heinrichsdorff P, Mao M H and Bimberg D 1999 Dephasing in InAs/GaAs quantum dots *Phys. Rev.* B **60** 7784–7
[12] Cusack M A, Briddon P R and Jaros M 1996 Electronic structure of InAs/GaAs self-assembled quantum dots *Phys. Rev.* B **54** R2300–3
[13] Pryor C 1999 Geometry and material parameter dependence of InAs/GaAs quantum dot electronic structure *Phys. Rev.* B **60** 2869–74
[14] Pryor C 1998 Eight-band calculations of strained InAs/GaAs quantum dots compared with one-, four-, and six-band approximations *Phys. Rev.* B **57** 7190–5
[15] Williamson A J and Zunger A 1999 InAs quantum dots: predicted electronic structure of free-standing versus GaAs-embedded structures *Phys. Rev.* B **59** 15819–24
[16] Shumway J *et al* 2001 Electronic structure consequences of In/Ga composition variations in self-assembled InxGa1-xAs/GaAs alloy quantum dots *Phys. Rev.* B **64** 125302
[17] Andreev A D, Downes J R and O'Reilly E P 2002 The effects of adjacent dislocations on the electronic and optical properties of GaN/AlN quantum dots *Physica* E **13** 1094–7
[18] Bastard G 1988 *Wave Mechanics Applied to Semiconductor Heterostructures* (New York: Halsted Press)
[19] Trellakis A and Ravaioli U 2001 Three-dimensional spectral solution of Schrödinger equation *VLSI Des.* **13** 341–7
[20] Lehoucq R B 2001 Implicitly restarted Arnoldi methods and subspace iteration *SIAM J. Matrix Anal. Appl.* **23** 551–62
[21] Li Y M *et al* 2001 Energy and coordinate dependent effective mass and confined electron state in quantum dots *Solid State Commun.* **120** 79–83
[22] Uskov A V, Magnusdottir I, Tromborg B, Mørk J and Lang R 2001 Line broadening caused by Coulomb carrier–carrier correlations and dynamics of carrier capture and emission in quantum dots *Appl. Phys. Lett.* **79** 1679
[23] Magnusdottir I 2003 Modeling of phonon- and Coulomb-mediated capture processes in quantum dots *PhD Thesis* Center for Optical Communication, Technical University of Denmark